Article

Optical Energy Increasing in a Synchronized Motif-Ring Array of Autonomous Erbium-Doped Fiber Lasers

José Octavio Esqueda de la Torre [1], Juan Hugo García-López [1,*], Rider Jaimes-Reátegui [1,*], José Luis Echenausía-Monroy [2], Eric Emiliano López-Muñoz [1], Héctor Eduardo Gilardi-Velázquez [3] and Guillermo Huerta-Cuellar [1,*]

[1] Optics, Complex Systems and Innovation Laboratory, Centro Universitario de los Lagos, Universidad de Guadalajara, Enrique Díaz de León 1144, Paseos de la Montaña, Lagos de Moreno 47460, Mexico; octavioesqueda@msn.com (J.O.E.d.l.T.); eemiliano.lopez@alumnos.udg.mx (E.E.L.-M.)

[2] Centro de Investigación Científica y de Educación Superior de Ensenada, Carretera Ensenada-Tijuana No. 3918, Zona Playitas, Ensenada 22860, Mexico; echenausia@cicese.mx

[3] Facultad de Ingeniería, Universidad Panamericana, Josemaría Escrivá de Balaguer 101, Aguascalientes, Aguascalientes 20296, Mexico; hgilardi@up.edu.mx

* Correspondence: jhugo.garcia@academicos.udg.mx (J.H.G.-L.); rider.jaimes@academicos.udg.mx (R.J.-R.); guillermo.huerta@academicos.udg.mx (G.H.-C.)

Abstract: This work investigates the enhancement of optical energy in the synchronized dynamics of three erbium-doped fiber lasers (EDFLs) that are diffusively coupled in a unidirectional ring configuration without the need for external pump modulation. Before the system shows stable high-energy pulses, different dynamic behaviors can be observed in the dynamics of the coupled lasers. The evolution of the studied system was analyzed using different techniques for different values of coupling strength. The system shows the well-known dynamic behavior towards chaos at weak coupling, starting with a fixed point at low coupling and passing through Hopf and torus bifurcations as the coupling strength increases. An interesting finding emerged at high coupling strengths, where phase locking occurs between the frequencies of the three lasers of the system. This phase-locking leads to a significant increase in the peak energy of the EDFL pulses, effectively converting the emission into short, high amplitude pulses. With this method, it is possible to significantly increase the peak energy of the laser compared to a continuous EDFL single pulse.

Keywords: optical energy; laser; network; ring; dynamics; phase-locking; coupling

1. Introduction

In recent years, the demand for high-power short-pulse lasers for various applications such as cutting, welding, surgery, material processing, photonic materials, and especially for optical communication has increased significantly [1–7] to maintain the transmission of the optical signal over a long distance without repetitive amplifiers. Recently, we were able to achieve giant pulses in the EDFL array by selectively controlling the multistability [8]. In addition, the temporal phase-locking among intensities of the lasers is considered one of the methods to generate high-energy ultrashort laser pulses, which can be either active or passive. Through this paper, we will refer to this technique as phase locking. Since 1964 [9], various phase-locking resonators have been developed for a fiber laser. These resonators require a complex, controllable amplitude and phase modulator. There are also several passive phase-locking techniques, such as a saturable semiconductor absorber [10,11], nonlinear polarization rotation [12,13], nonlinear optical loop mirror [14] and nonlinear amplifier loop mirror [15].

Among the different types of fiber lasers, EDFLs stand out from other devices due to their advantages in applications for optical information transmission systems, as their

implementation and optical components are small and their handling is simple; The laser emission of an EDFL is at 1550 nm, which is optimal for communication applications due to the low absorption of this type of radiation in the optical fibers [16], and; some results show that EDFLs exhibit rich dynamic behavior, including period doubling, chaos, and multistability [17,18]. As mentioned above, EDFLs have some properties known for use in optical communication [3,19], but also other applications, such as optical coherence tomography [20], spectral interferometry [21], optical metrology [22], optical sensor technology [23], industrial micromachining [24], LIDAR systems [25] and medicine [26].

Isolated oscillators follow a simple path in phase space. When two or more of these systems are connected, the probability of possible complex behaviors becomes high and the equations that define their behavior become intractable. Every oscillator is only able to interact with a limited number of nearby neighbors. [27]. When considering different coupled network structures [28], the connection of three nodes in a ring arrangement is of particular interest as it could allow the occurrence of a phenomenon called rotating phase oscillations (RPO) along the coupled nodes [29–32]. This oscillation phenomenon was first described on the basis of results in ring reactors of reaction-diffusion systems [33,34]. In 1966, Nekorkin and others showed the phenomenon of traveling oscillations in a ring of connected bistable systems that preserve sinusoidal nonlinear dynamics [35]. It is important to emphasize that unidirectional coupling is particularly important as It enables the transmission of a signal from one subsystem to another without receiving any feedback. In particular, unidirectional coupling in motif-ring arrays has been found to induce phase synchronization, which leads to a significant increase in peak pulse energy through mechanisms such as Q-switching [36]. In addition, unidirectional coupling is often used in electrical systems based on the models of Duffing [37], Chua [38] and Lorenz [39,40], where RPO was obtained. As the coupling strength changed, rings of unidirectionally coupled oscillators showed an evolution from stable equilibrium to quasiperiodicity. Subsequently, there is a change to chaos and hyperchaos as in the Rulkov [41], Duffing [42] and Lorenz [39,43] oscillator results.

However, one of the challenges is to increase the optical energy output of EDFLs without introducing external modulation, which can complicate system design and reduce reliability. A promising approach to overcome this challenge is the synchronization of multiple EDFLs in a motif array configuration [8]. This work investigates the potential to increase the optical energy in a coupled motif-ring array of autonomous EDFLs by carefully tuning the coupling strength between the lasers. To achieve this, we analyze the evolution of the behavior in the system using different characterization techniques based on the study of the obtained time series. In previous results, Barba-Franco et. al. have shown that the dynamics of this three-ring node network, while similar to other coupled systems, still exhibit unique properties specific to laser systems [42].

The organization of this paper is: The model of a single EDFL without pump modulation is described in detail in Section 2. Section 3 outlines the model for three ring-connected EDFLs. Section 4 analyzes the resulting energy and the phase-locking phenomenon as an advantage to synchronize the laser's emission. The main conclusions are presented in Section 5.

2. Autonomous EDFL Model

The emission of a single-mode laser is described by three differential equations, where the primary state variables are the optical field, the population inversion and the polarization. The decay rates of these variables differ depending on the laser type (A, B or C). If the value of one variable is significantly greater than the others, it decays faster, which allows the equations to be simplified. For class A lasers, the population inversion and polarization decay quickly in relation to the optical field. For class B lasers, only the polarization decays quickly. For class C lasers, all three variables have similar decay rates. Consequently, the solution to the equations for Class A lasers is a single stable fixed point. For Class B lasers, the solution is a fixed focal point that attracts the phase trajectory in the optical field

and population inversion space, leading to relaxation oscillations. Class C lasers exhibit undamped periodic or non-periodic (chaotic) pulsations. In addition, Class B lasers may exhibit periodic or chaotic oscillations when subjected to periodic external forces or delayed feedback on any of the laser parameters or variables.

The EDFL discussed in this paper is classified as a class B laser, similar to solid-state lasers, semiconductor lasers and externally discharged gas lasers (such as CO_2 and CO lasers) [44]. The basic dynamic properties of the EDFL are very similar to those of other class B lasers. In particular, the polarization is adiabatically eliminated and the laser dynamics is described by two rate equations for the field and population inversion, with multiple routes to chaos identified. However, despite the extensive research on EDFLs, the dynamics of networks of coupled EDFLs has not yet been thoroughly explored.

To know what the dynamics of the laser-pumped EDFL looks like, a power balance approach is used that takes into account the excited state absorption (ESA) in erbium at the 1.5-μm wavelength and averages the population inversion along the pumped active fiber. This model accounts for key factors such as the ESA at the laser wavelength and the depletion of the pump wave as it propagates along the active fiber, resulting in undamped self-oscillations in the laser that are observed experimentally without external modulation [18,45,46]. The balance equations for the laser power P (the sum of the powers of the counterpropagating waves inside the cavity, measured in s^{-1}) and the averaged population y of the upper level (a dimensionless variable, $0 \leq y \leq 1$) are defined as follows.

$$\dot{P} = \frac{2L}{T_r} P \{ r_w \alpha_0 (N[\xi - \eta] - 1) - \alpha_{th} \} + P_{sp}$$
$$\dot{N} = -\frac{\sigma_{12} r_w P}{\pi r_0^2}(\xi N - 1) - \frac{N}{\tau} + P_{pump}. \tag{1}$$

In this context, L refers to the length of the erbium-doped fiber (EDF), and $T_r = \frac{2n_0(L+l_0)}{c}$ represents the photon lifetime within the cavity, where l_0 takes into account the tails within the cavity of the fiber Bragg grating couplers (FBG). The variable P corresponds to the laser emission within the cavity and serves as an initial condition. The other parameters in the Equation (1) include $r_w = 1 + \exp\left[2\left(\frac{r_0}{w_0}\right)^2\right]$, a factor that quantifies the match between the fundamental mode of the laser and the erbium-doped core volumes within the active fiber, where r_0 is the fiber core radius and w_0 is the radius of the fundamental mode of the fiber. The small-signal absorption of the erbium fiber at the laser emission wavelength is denoted by $\alpha_0 = N_0 \sigma_{12}$, where $N_0 = N_1 + N_2$ is the total number of erbium ions in the active fiber. The population N of the upper laser level 2 is expressed as:

$$N = \frac{1}{n_0 L} \int_0^L N_2(z) dz, \tag{2}$$

here N_2 denotes the inversion of population of the upper laser level "2", and n_0 is the refractive index of a "cold" EDF core. The coefficient in brackets represents the ratio between the cross-section absorption in the excited state (ESA) σ_{23} and the absorption cross-sections in the ground state at the laser wavelength. More precisely: $\xi = \frac{\sigma_{12} + \sigma_{21}}{\sigma_{12}} = 2$ and $\eta = \frac{\sigma_{23}}{\sigma_{12}}$. It is important to note that the cross-section σ_{12} of the return stimulated transition has almost the same energy. The cavity loss parameter is given by α_{th} and is defined as $\alpha_{th} = \gamma_0 + \frac{1}{2L} \ln\left(\frac{1}{R}\right)$ at the initial lasing, where γ_0 corresponds to the non-resonant fiber loss and R is the reflection coefficient of the FBG couplers. The spontaneous emission into the fundamental laser mode is defined as

$$P_{sp} = \frac{10^{-3} N}{\tau T_r} \left(\frac{\lambda_g}{w_0}\right)^2 \frac{r_0^2 \alpha_0 L}{4\pi^2 \sigma_{12}} \tag{3}$$

for which τ, given in seconds, is the time duration of the erbium ions in state 2 and λ_g is the laser wavelength. Finally, the pump power P_{pump} is defined as

$$P_{pump} = P_p \frac{1 - \exp[-\beta\alpha_0 L(1 - N)]}{n_0 \pi r_0^2 L}, \tag{4}$$

where P_p stands for the light emitted by a pump laser diode at the fiber input and the parameter $\beta = \alpha_p/\alpha_0$ defines the relationship between the absorption coefficients of the erbium fiber at the pump wavelength λ_p and the laser wavelength λ_g. In this study, the laser spectrum has a width equal to 10^{-3} of the spectral bandwidth of erbium luminescence. It should be noted that Equation (1) represents an autonomous EDFL, which operates in a fixed-point regime.

The given model uses parameters feed from real values corresponding to an experimental EDFL with an active EDF. In this case, the EDF has a length $L = 80$ cm [47]. Another parameter for which real values are used is the refractive index $n_0 = 1.45$, the tails inside the cavity $l_0 = 20$ cm, the time a photon remains in the laser cavity $T_r = 8.7$ ns, the half of the fiber core diameter $r_0 = 1.5$, cm and the half of the diameter of the fundamental fiber core $w_0 = 3.5 \times 10^{-4}$ cm. The last value was measured experimentally and was slightly higher than 2.5×10^{-4} cm, which is derived from the definition for single-mode fiber with step index $w_0 = r_0(0.65 + 1.619/V^{1.5} + 2.879/V^6)$, with the parameter V, that refers to the numerical aperture NA and r_0 as $V = 2\pi r_0 NA/\lambda_g$, with the values r_0 and w_0 results in $r_w = 0.308$.

Table 1, presents the coefficients that characterize the resonance absorption properties of the erbium-doped fiber at both laser and pump wavelengths for a heavily doped fiber with an erbium concentration of 2300 ppm.

Table 1. Coefficients used in numerical simulations.

Coefficient	Value	Coefficient	Value	Coefficient	Value
α_0	0.4 cm^{-1}	β	0.5	σ_{12}	2.3×10^{-21} cm^2
ξ	2.0	η	0.4	σ_{21}	2.3×10^{-21} cm^2
τ	10^{-2} s	γ_0	0.038	σ_{23}	2.3×10^{-21} cm^2
R	0.8	α_{th}	0.6×10^{-21} cm^2	λ_g	1.56×10^{-4} cm

Finally, the emission wavelength $\lambda_g = 1.56 \times 10^{-4}$ cm ($h\nu = 1.274 \times 10^{-19}$ J) and this value is given by the one experimentally obtained, with the maximum reflection coefficients of both fiber Bragg gratings (BGs) centered on this wavelength, as shown in [48]. The pump parameters are the excess of the laser threshold ε, which is defined as $P_p = \varepsilon P_{th}$, where the pump power of the threshold is

$$P_{th} = \frac{N_{th}}{\tau} \frac{n_0 L \pi w_p^2}{1 - \exp[-\alpha_0 L \beta(1 - N_{th})]} \tag{5}$$

and the threshold population of the level "2"

$$N_{th} = \frac{1}{\xi}\left(1 + \frac{\alpha_{th}}{r_w \alpha_0.}\right) \tag{6}$$

By numerical simulation of Equation (1), the time series data show the evolution of the dynamics in the EDFL. To simulate the behavior of the laser, parameters were used that are very close to those of the experimental setup described in [49]. Here, a pump power of $P_p^0 = 7.4 \times 10^{19}$ s^{-1} was chosen, which corresponds to the value required to achieve a relaxation oscillation frequency of the laser of $f_0 = 28.724$ kHz, as shown in the time series

and Fourier spectrum in Figure 1 (left) and Figure 1 (right) respectively. The solution of the laser Equation (1) is a stable fixed point.
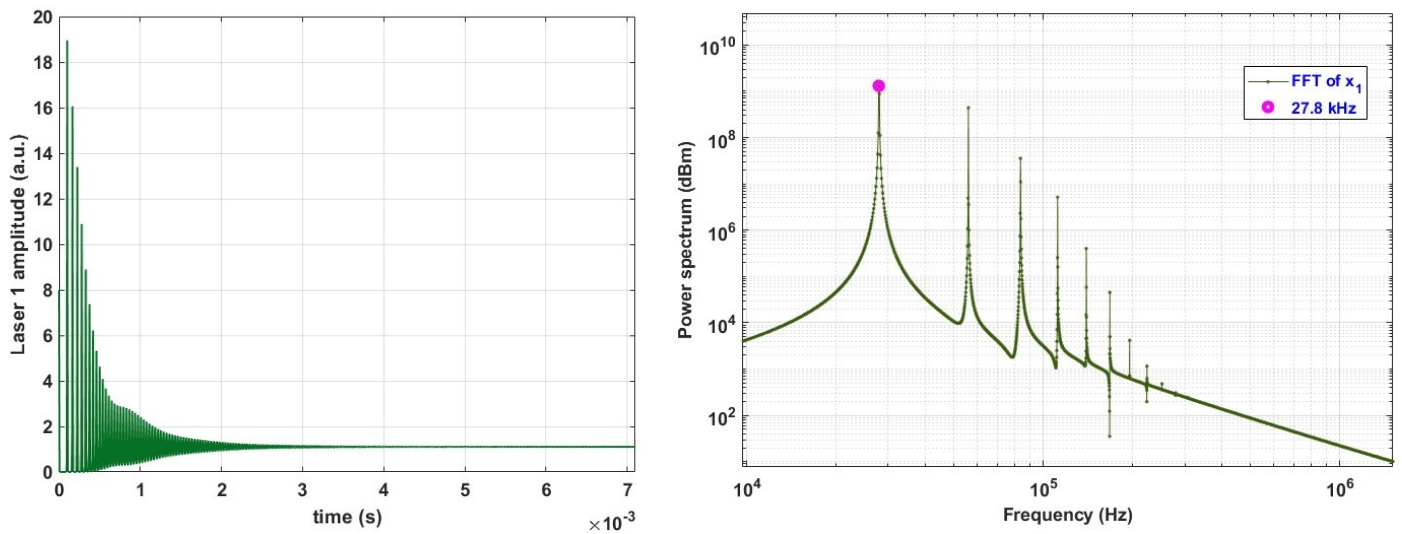

Figure 1. Each laser shows a (**left**) time series of the relaxing oscillation and (**right**) the corresponding relaxation frequency f_r for the autonomous EDFL described by the Equation (1).Original data obtained from the numerical simulation of our experiments please see Supplementary Materails.

3. Evolution of the System to Achieve Stable Energy

Ring-shaped connected systems can be understood as a cyclic sequence of interactions [50]. Even for simple network motifs consisting of only three oscillators, there are thirteen ways in which they can be coupled [51]. As mentioned above, in this work we focus on studying the energy of the simplest network of three unidirectionally coupled EDFLs, and its evolution while the coupling strength k increases where each laser injects radiation into the next device in the link, as shown in the schematic representation in Figure 2. The lasers studied have no modulation and are therefore in a fixed-point regime with minimum energy, but by increasing the coupling between the lasers in the ring it is possible to observe different behaviors before obtaining a signal with stable energy many times greater than the initial energy. The following pages explain how the system behavior develops until a maximum energy value is reached. Using the normalized equations from Equation (1) as presented in [52,53], the dynamic behavior of this ring is described by the following differential equations for the laser intensity x_j ($j = 1, 2, 3$) and the population inversion y_j (Equations (7) and (8)):

$$\frac{dx_j}{dt} = ax_jy_j - bx_j + c(y_j + 0.3075) \tag{7}$$

$$\frac{dy_j}{dt} = dx_jy_j - (y_j + 0.3075) + P_{pmod_j}\left(1 - e^{-18\left(1 - \frac{1-(y_j+0.3075)}{0.6150}\right)}\right) \tag{8}$$

with pumping

$$P_{pmod_j} = 506(1 + k(x_{j-1} - x_j)) \tag{9}$$

with $0 < k < 0.20$ as the coupling coefficient, having $a = 6.620 \times 10^7$, $b = 7.4151 \times 10^6$, $c = 0.0163$, and $d = 4.0763 \times 10^3$. The lasers are coupled in a diffusive form which means that for laser 1 We add a term $k * (x_2 - x_1)$, as Equation (9) mentions, which means that laser 1 is coupled with laser 2, and "k" is the coupling strength. Similarly, the coupling between laser 2 with laser 3, and laser 3 with laser 1 is implemented. Also, We must consider that a change in the parameter k directly affects the pump power, then the behavior of the system could change after a threshold value for k.
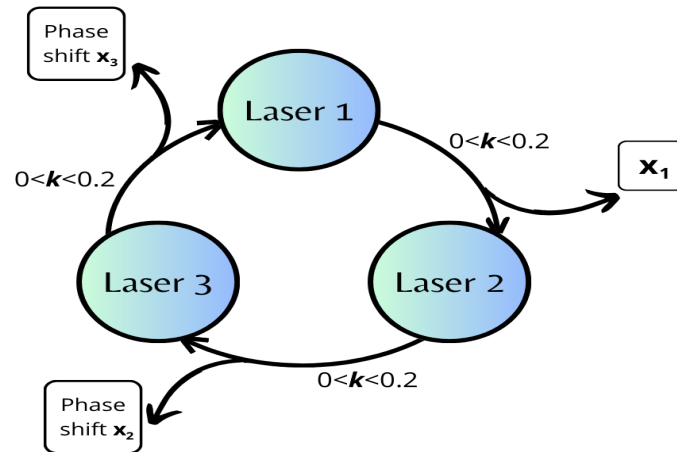
Figure 2. Schematic arrangement of a three EDFL in a ring connection with phase shift for laser 2 and laser 3.

Due to the symmetry of the ring configuration, the behavior of each EDFL follows the same dynamics. Therefore, we show in Figure 3 (top) the dynamic evolution of one of the lasers in the ring (x_1), and Figure 3 (bottom) shows λ, the maximum Lyapunov exponent (MLE), as a function of the coupling k between the lasers. The bifurcation diagram shows the Landau path leading from a stable fixed point to a chaotic behavior through a quasi-periodicity regime characterized by different Hopf bifurcations [54,55]. This scenario was identified by Newhouse, Ruelle, and Takens (known as the NRT scenario [56]), who found that a chaotic attractor resembling a 3D torus forms shortly after the third Hopf bifurcation. Our model, which is described by Equations (7) and (8), shows a similar hyperchaotic behavior when the coupling strength k is varied.
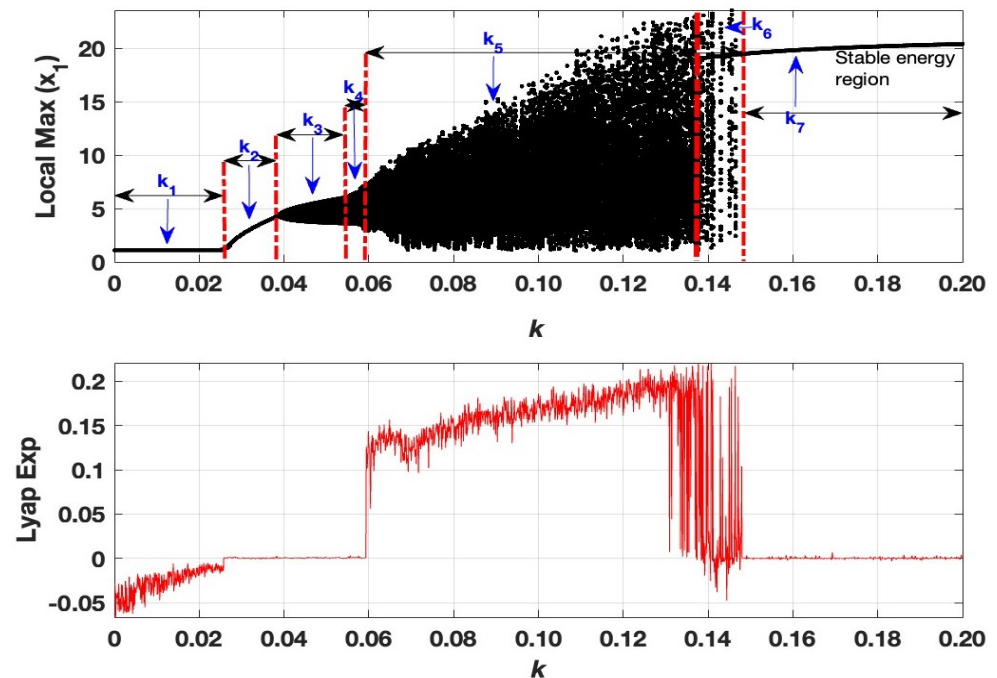

Figure 3. (**Top**) Bifurcation diagram of the time-series peak energy of an EDFL (x_1 (in arbitrary units), showing the dynamic evolution of each laser in the ring configuration as the coupling k increases, and (**button**) the MLE as a function of k.

To confirm the dynamic evolution of the coupled oscillators in Figure 3, the time series and Poincaré sections are shown in Figure 4, which illustrate the dynamic transitions when the system moves from a constant fixed point to chaotic dynamics. The Poincaré section is particularly useful for identifying patterns like limit cycles or chaotic behavior in systems of oscillators, especially when studying nonlinear differential equations. For a limit cycle behavior, only one point is identified in the Poincaré section, when dynamics is a 2D torus, the Poincaré section shows a closed loop, for a 3D torus two closed cycles will be shown, and for chaotic behavior, it will show a cloud of points. For the three lasers system, when the coupling strength increases from the initial value k to ($k_1 \approx 0.0258$), the equilibrium (Figure 1) undergoes a Hopf bifurcation and evolves into a periodic oscillation (Figure 4a), with the MLE tending towards zero. This periodic behavior is maintained within the narrow range ($0.0258 < k < 0.0381$). At ($k_2 = 0.0382$), the limit cycle changes to a quasi-periodic state (2D torus), as shown in Figure 4b, which occurs when the MLE reaches zero. If (k) continues to increase, a 3D torus appears at ($k_3 = 0.0549$) (Figure 4c), marked by the MLE reaching zero This regime remains within the interval ($0.0549 < k < 0.0583$). When (k) reaches ($k_4 = 0.0584$), the system becomes chaotic (Figure 4d), as the MLE becomes positive. A further increase in the coupling strength finally leads to the system returning to a stable limit cycle at ($k_7 = 0.1481$) (Figure 4e), which is indicated by the MLE returning to zero. The region shown in (Figure 3a) as k_6 corresponds to a region for which we can obtain a coexisting chaos and stable oscillation. Next Table 2 shows the relationship between the results in Figure 4 with the analyzed behaviors using the Poincaré section, and power spectrum, explained in the following sections.

Table 2. Evolution of the systems as a function of k.

| k_n	Range	Behavior	Description
k_1	$0.0000 \leq k \leq 0.0258$	Fixed point	Shows the natural frequency of the system (Figure 1)
k_2	$0.0258 < k \leq 0.0381$	Periodic oscillation	A dot in Poincaré section, Figure 4a(ii), show a peak in frequency (Ω_0) Figure 7a
k_3	$0.0381 < k \leq 0.0549$	2D Tourus	A closed trajectory in Poincaré section, Figure 4b(ii), show two peaks in frequency (Ω_0, Ω_1) Figure 7b
k_4	$0.0549 < k \leq 0.0583$	3D Tourus	Double closed trajectory in Poincaré section, Figure 4c(ii), show three peaks in frequency ($\Omega_0, \Omega_1, \Omega_2$) Figure 7c
k_5	$0.0583 < k \leq 0.1300$	Chaos	A dot cloud in Poincaré section, Figure 4d(ii), show wide spectrum frequency, Figure 7d
k_6	$0.1300 < k \leq 0.1481$	Chaos + Fixed point	Coexistence of chaos and periodic behavior
k_7	$0.1481 < k \leq 0.2000$	Stable limit cycle	A dot in Poincaré section, Figure 4e(ii) high energy, high frequency
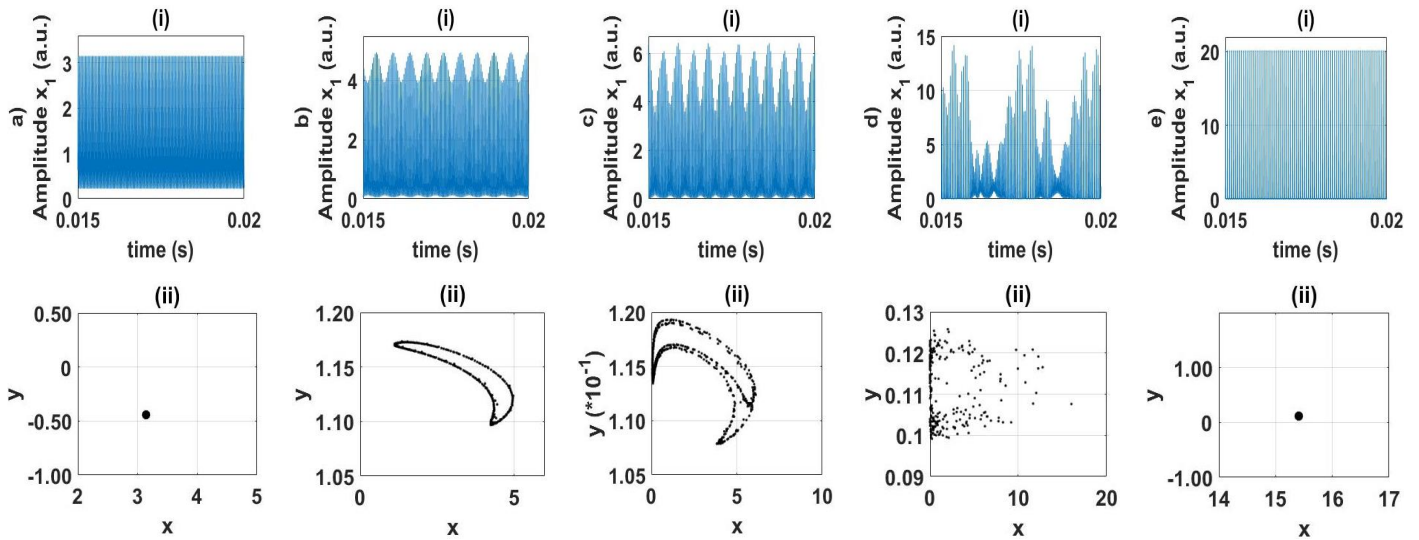
Figure 4. (**i**) Time series and (**ii**) the corresponding Poincaré sections at (**a**) $k = 0.0258$, (**b**) $k = 0.0382$, (**c**) $k = 0.0549$, (**d**) $k = 0.0584$, and (**e**) $k = 0.1481$.

3.1. Rotating Phase Oscillations

Now, consider an intriguing phenomenon known as *rotating phase oscillations* (RPO). As can be observed in Figure 4b–d, the time series shows a slow envelope (which can be periodic, quasi-periodic or chaotic). These low-frequency oscillations arise from an RPO (also periodic, quasi-periodic or chaotic) that propagates along the ring of unidirectionally coupled oscillators and is driven by the phase difference between the high-frequency oscillations of the individual lasers. The RPO phenomenon was first observed in a ring of coupled Chua oscillators [57,58] and later also in ring arrays of coupled Lorenz oscillators [43,59] and also in Duffing systems [37,60,61]. The RPO has a similar effect to external modulation and favors the oscillation in a low-frequency regimen [62]. For the case of a shift in frequency due to the change of k causes the interaction between the periodic rotating wave and the local oscillation of each laser, a dynamic behavior corresponding to a local 2D torus in which the RPO produces a quasi-periodic behavior (as shown in Figure 4c). If the coupling strength k increases a little further, the local 2D torus mixes with the quasi-periodic RPO, (Figure 4d) shows resulting in the formation of a local 3D torus. With a further increase in k, the rotating wave begins having interaction with the local 3D torus, and then a chaotic behavior results (Figure 4e). If the coupling is stronger than $k = 0.0381$, the rotating wave finally interacts with the chaotic dynamics and the chaotic trajectory stabilizes in a limit cycle. For higher values of k, the limit cycle is maintained. It can be observed that the ring system eventually generates momentum as a saturable absorber after developing different dynamical behaviors.

In oscillating modes, it can be seen that the time series of all oscillators vary only in phase, leading to phase shifts at each subsequent node and generating a phase wave that rotates through the cyclic ring. The wave dynamics for rings with 3 lasers are shown in Figure 5 for four different values of the coupling strength: $k = 0.0257$, $k = 0.0381$, $k = 0.0548$ and $k = 0.0583$. In the upper part, the time series patterns for all oscillators are shown, where the rotating waves manifest themselves as oblique stripes. The phase waves traveling along the ring of oscillators are visible. The bottom row shows the phase portraits of the corresponding laser, which are the same for all oscillators due to their identical nature. Here, we can see that the size of the attractor increases as the coupling strength increases.
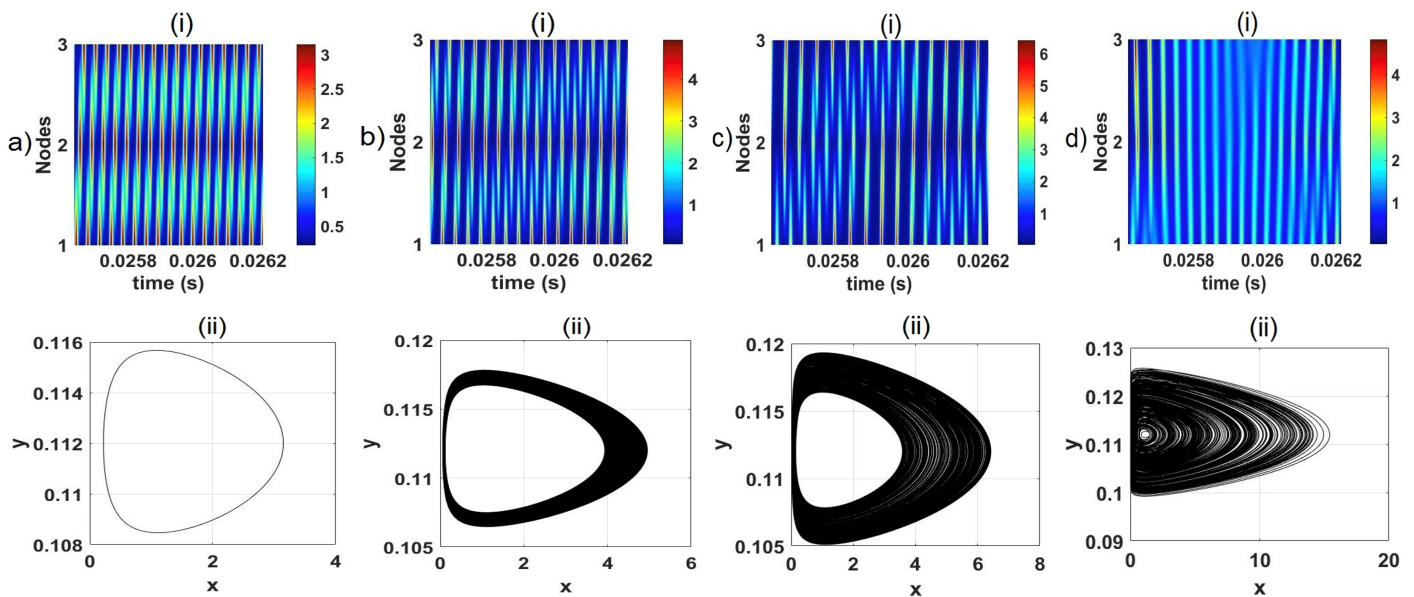
Figure 5. (**i**) Rotating phase oscillations and (**ii**) phase portraits for (**a**) $k = 0.0257$, (**b**) $k = 0.0381$, (**c**) $k = 0.0548$ and (**d**) $k = 0.0583$.

3.2. Frequency Spectrum Analysis

The study of the fast Fourier transform (FFT) complements traditional qualitative and quantitative tools in dynamical systems, such as Poincaré maps, bifurcation diagrams of local maxima, and Lyapunov exponents. FFT spectral analysis is a powerful technique in science and engineering to study the dynamics of systems [63,64].

Figure 6 shows the bifurcation diagram of the evolution of the frequency-power spectrum of x_1 as a function of the coupling strength k. When k_1 appears, it means that the dynamic behavior changes by a Hopf bifurcation as shown in (Figure 6), there is a system that shifts from a steady-state to a periodic solution, and the initial oscillation frequency Ω_0 appears as a distinct peak in Figure 7a. At k_2 the second Hopf bifurcation occurs. Now we see the occurrence of two different or incommensurable frequencies, Ω_0 and Ω_1, which generate the 2D torus dynamics. (see Figure 7b). The 2D torus persists until the next Hopf bifurcation at k_3, where the system transitions from a 2D torus to a quasi-periodic solution with three frequencies (3D torus). At this 3D torus, a third independent frequency Ω_2 appears in the power spectrum (see Figure 7d). The 3D torus is predominant in the range $k_3 < k < k_4$. If the coupling strength $k_3 < k < k_4$ is increased further, the frequency interactions lead to the annihilation of the 3D torus behavior, resulting in a broad frequency spectrum that leads to chaotic dynamics for $k_4 < k < k_5$. This chaotic behavior is manifested in the FFT spectrum by various randomly distributed frequency peaks with different amplitudes. Similar phenomena when examining other oscillators in the same ring arrangement. For example, Sánchez et al. [43] observed RPO in a ring of unidirectionally coupled Lorenz oscillators while studying the evolution from an RPO to a chaotic rotating wave through quasi-periodicity. Subsequently, in [65], the authors explained the phenomenon of RPO in a ring of seven unidirectionally coupled Duffing oscillators using FFT bifurcation analysis.
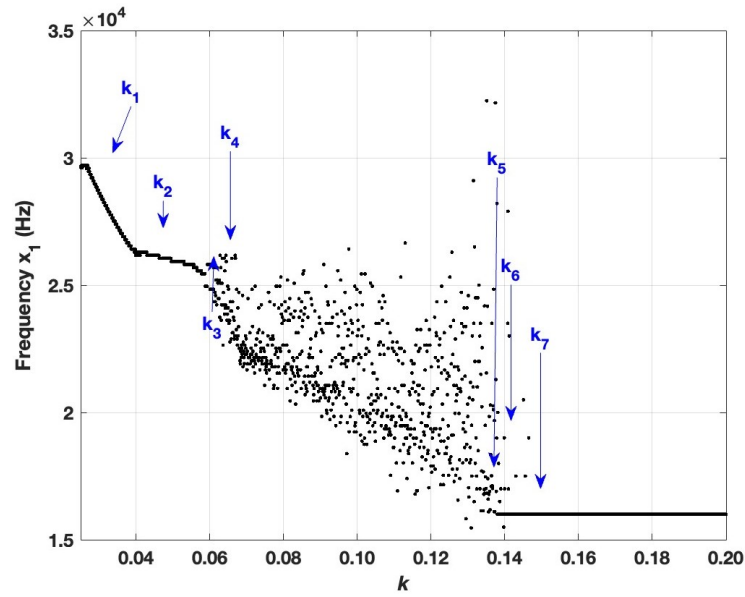
Figure 6. Bifurcation diagram showing the development of the frequency-power spectrum of x_1 as a function of the coupling strength k.
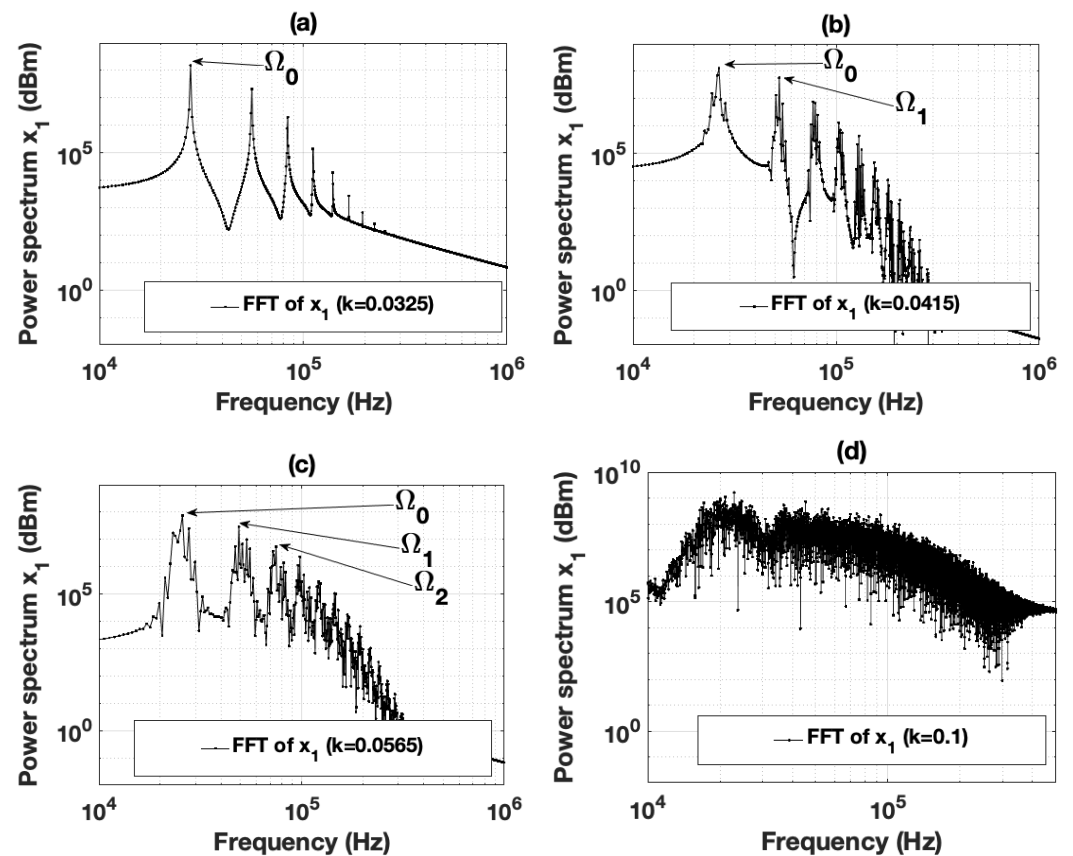

Figure 7. Power spectrum at (**a**) $k = 0.0325$ $\Omega_0 = 28$ kHz, (**b**) $k = 0.0415$, $\Omega_0 = 52.32$ kHz, $\Omega_1 = 25.83$ kHz, (**c**) $k = 0.0565$, $\Omega_0 = 25.83$ kHz, $\Omega_1 = 49.01$ kHz, $\Omega_2 = 74.83$ kHz, and (**d**) $k = 0.1$.

3.3. Coexistence of Attractors

Another phenomenon that occurs when studying the evolution of this system is the coexistence of attractors. As already mentioned, when the chaotic behavior ends and the final stable dynamics appear, two different behaviors can be seen in the transition when $k_5 < k < k_6$. In Figure 3 for $k < 0.14$ we see the born stable energy region surrounded by

chaotic behavior. The phase space and power spectra of these coexisting regimes are shown in Figure 8 for $k = 0.1408$, for which one can identify the periodic and chaotic behavior. By using fractional-order calculus tools, similar multistable dynamics were observed by Barba et al., who studied a motif of three double-well Duffing oscillators [66]. By randomly changing the initial conditions of their system, they observed the coexistence of stable fixed points, limit cycles, 2D and 3D tori, and chaos for certain fractional order indices and coupling strengths. In particular, for the region $0.13 < k_6 < 0.1481$, the dynamical behavior of a stable limit cycle exists in the same region where chaos exists (see bifurcation diagram in Figure 3). In this system, chaotic and periodic orbits interact with the rotating wave, leading to a monostable limit cycle. Similar results were explained by other researchers (e.g., [67,68]), where a periodic perturbation was used to generate multistable dynamics Here, the rotating wave serves as this secondary perturbation, which significantly increases the power of the laser pulses and causes the lasers to operate in a Q-switching mode with short high-amplitude pulses.
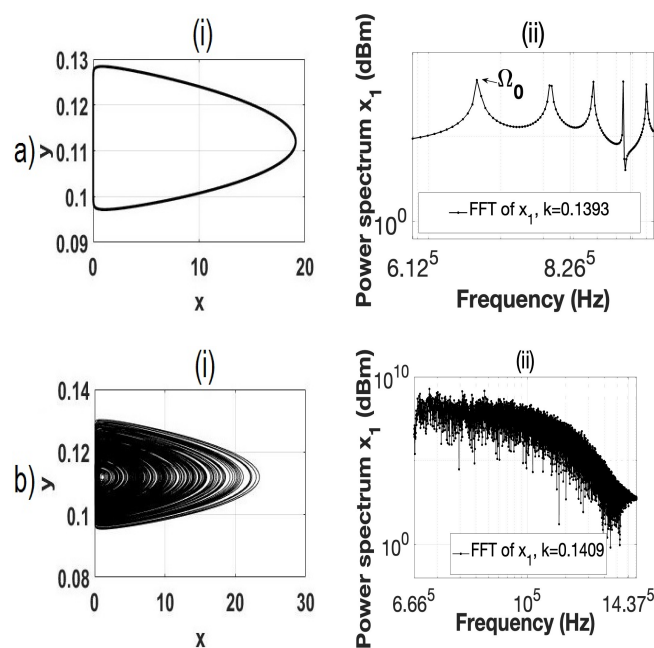

Figure 8. Bistable region for $k = 0.1409$ containing (**a**) a stable limit oscillation and (**b**) chaotic dynamics for (**i**) the phase spaces of the behavior and (**ii**) the frequency-power spectra.

4. Increase of the Optical Pulse Energy Through Synchronized Phase-Looked EDFLs

After $k = 0.1481$ the dynamic behavior obtains a stable oscillation for all lasers in the ring. Now we can observe temporal series with the same energy intensity for all lasers in the system and with a constant phase difference between them. This phenomenon is called *phase − locking* and occurs due to the interaction of the oscillators in the ring configuration [39,40]. This phase discrepancy arises from the sequential nature of the light propagation of the system, where each signal experiences a time delay with respect to the others. We have numerically investigated the strength and direction of the relationship between x_1, x_2 and x_3 using the cross-correlation function, which is represented as follows:

$$R_{x_1,x_2}(\tau) = \mathbb{E}[x_1(t)x_2(t + \tau)] \tag{10}$$

where $x_1(t)$ and $x_2(t)$ are the signals to be compared, which correspond to the individual oscillators, $\mathbb{E}$ denotes the expected value and τ is the time lag between the peak values. With this function, we can quantify the difference between the signals and determine their relative phase shifts. Figure 9 shows on the left side the time series of the three coupled lasers obtained after $k = 0.1481$, and we can see that the phase difference is constant (phase-locking), which is confirmed by using the Equation (10). On the right side of Figure 9 we

can see the temporal series corresponding to the laser of the ring adding a phase shift, then the phase difference is reduced to zero.
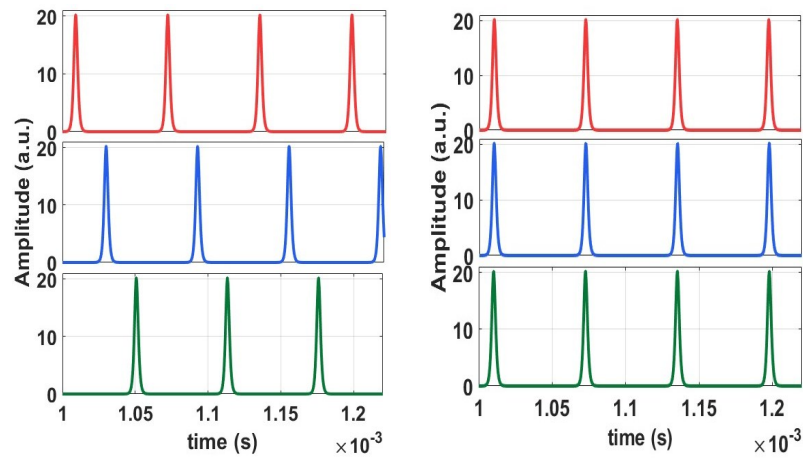

Figure 9. Temporal oscillations of the three lasers in the ring (laser 1 in red, laser 2 in blue, and laser 3 in green), in the left figure it is possible to appreciate the phase-locking between the lasers, and at the right the temporal series with phase-shifting to synchronize the pulses.

From the result obtained using the cross-correlation function, we can calculate the phase difference to prove the phase shift with the following relations

$$\phi_{ij} = arctan\left(\frac{y_{ij}^{\bullet}}{x_{ij}}\right) \tag{11}$$

$$\theta_{ij} = \phi_i - \phi_j. \tag{12}$$

Our analysis reveals complex interaction patterns in which the correlation varies significantly with time and optical transmittance. Figure 10 shows the phase difference between laser 1 and laser 2, which is given in radians. The corresponding difference between laser 2 and laser 3 as well as laser 3 and laser 1 is the same.
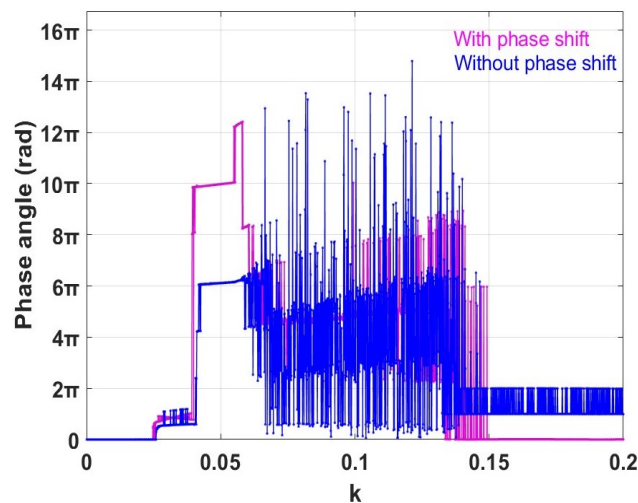

Figure 10. Phase difference between the obtained laser energy for $k > 0.1481$ without phase correction (blue), and with phase correction (pink). $0 < k < 0.2$.

Figure 11 shows the phase synchronization scenarios resulting from Equations (12) and (11). Here we show how the time-averaged phase synchronization depends on the coupling strength k. We can also observe how the phase difference changes when applying phase correction calculations. Figure 11a shows the phase relationship between the signals x_1 and

x_2 without any phase modification. In contrast, Figure 11b shows the phase behavior after applying a cross-correlation function to x_2 to align it with the signal x_1.
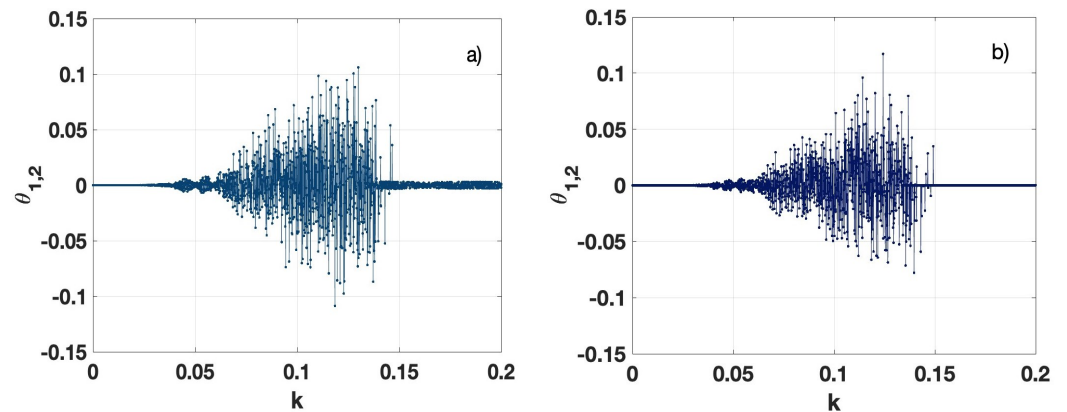

Figure 11. Averaged phase synchronization compared to the optical transmittance k for x_1 and x_2 (**a**) with and (**b**) without phase shift.

In the latter case, the phase difference approaches zero beyond $k = 0.15$. This shows that the systems are phase-coupled at optical transmittance values exceeding this threshold. Consequently, their signals can be summed, resulting in a significant increase in optical power. Figure 12a shows the bifurcation diagram of the superposition of the three lasers connected in the ring. For $k > 0.15$, the result of each coupled laser energy has a value of 20 (a.u.), which represents the individual energy of each laser and is twenty times higher than the initial value at the low coupling. However, when the phase shift was applied, there was a larger increase in optical energy to 60 (a.u.) as shown in Figure 12b.
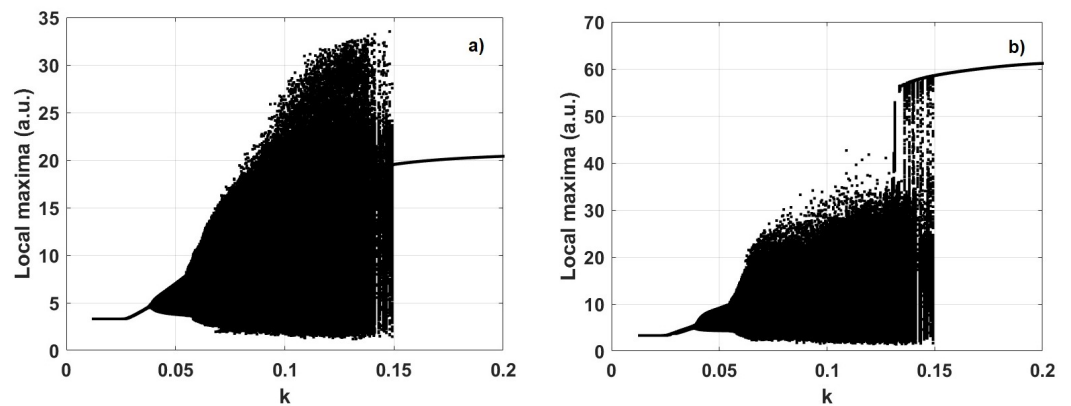

Figure 12. Bifurcation diagrams of the peak intensity of the superposition of x_1, x_2 and x_3 (**a**) without phase shift and (**b**) with phase shift, for $k = 0.18$.

The corresponding time series of the total energy that can be obtained by adding the individual laser energy for $k > 0.15$, taking into account the case without phase shift and the case with phase shift, can be seen in Figure 13. The differences between them are the oscillation frequency and the pulse intensity. In both cases, the increase in optical energy compared to the initial energy is evident and is achieved by increasing the coupling between the oscillators.
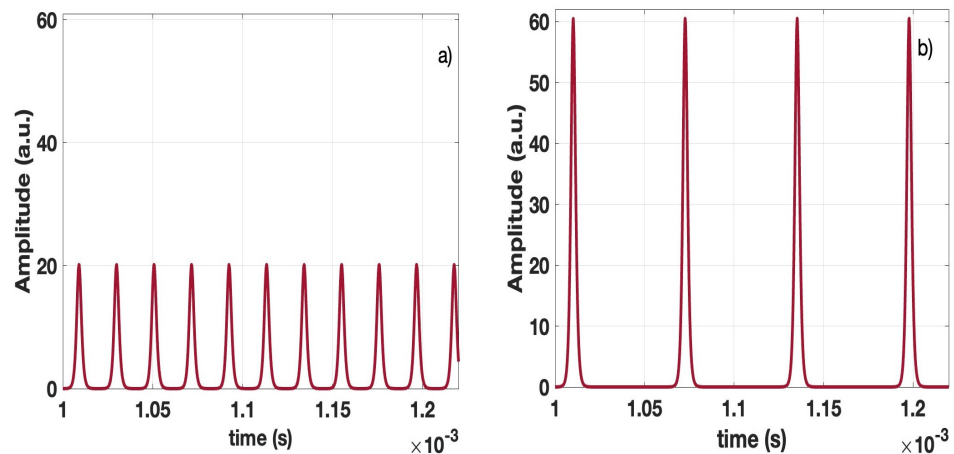
Figure 13. (**a**) Time series of x_1, x_2, x_3 and the sum of these three intensities ($x_1 + x_2 + x_3$) without phase shift for $k = 0.18$ and (**b**) time series of x_1, x_2, x_3 and the sum of these three intensities ($x_1 + x_2 + x_3$) with phase shift for $k = 0.18$.

5. Conclusions

In this study, we performed a numerical analysis of three unidirectionally coupled ring EDFLs, focusing on how the energy in the system increases at high coupling after a system´s evolution with rich, dynamic behavior. Using a mathematical model with three variables representing the laser intensities and three variables for population inversions across all lasers, we studied the transition of the system from stable equilibrium to a stable high-energy state within the ring. The analysis was performed using time series, bifurcation diagrams, power spectra, Poincaré sections, and Lyapunov exponents. The results show that the system enters chaos through a Hopf bifurcation followed by a torus bifurcation. Depending on the strength of the coupling, the RPO through the ring can exhibit periodic, quasi-periodic or chaotic behavior.

The research discovered that periodic and chaotic orbits can coexist within a specific range of coupling strengths as the laser coupling intensifies. This bi-stable behavior decreases with a further increase in coupling strength, leading to a mono-stable system characterized by a single limit cycle within a stable energy range. The stabilization is due to the interplay between chaotic and periodic orbits with the rotating wave, which functions as a secondary sinusoidal disturbance that ultimately removes the chaotic attractor.

A particularly significant result was observed under strong coupling conditions, where phase-locking leads to a substantial rise in the peak power of the laser pulses. At coupling strengths greater than ($k > k6$), all EDFLs operate in pulsed mode and generate short pulses with high amplitude. This model has great potential for applications that require huge laser pulses. In this study, we achieved nearly twenty-fold increase in peak pulse power compared to the continuous mode for each laser, in contrast, when the lasers remain uncoupled. With a zero phase difference by summing intensities, the lasers can increase the output power by almost 60 times when coupled. This significant improvement is crucial for optical communication, as optical signals transmitted over long distances through optical fibers are significantly attenuated. With optical amplifiers that take advantage of the nonlinear properties of EDFLs, high performance can be achieved in optical signal transmission. In these instances, the coexistence of pulsed regimes with varying pulse amplitudes and managed bi-stability can be advantageous for producing high-power laser pulses.

However, this study has some limitations. We focused on the simplest configuration—a ring with only three lasers—which limits the generalizability of our results to more extensive laser networks. Nevertheless, some dynamic behaviors that we observed in our system may also be relevant for more extensive networks, pointing to a promising direction for future research.

References

1. Zervas, M.N.; Codemard, C.A. High power fiber lasers: A review. *IEEE J. Sel. Top. Quantum Electron.* **2014**, *20*, 219–241. [CrossRef]
2. Digonnet, M.J. *Rare-Earth-Doped Fiber Lasers and Amplifiers, Revised and Expanded*; CRC Press: Boca Raton, FL, USA, 2001.
3. Luo, L.; Chu, P. Optical secure communications with chaotic erbium-doped fiber lasers. *JOSA B* **1998**, *15*, 2524–2530. [CrossRef]
4. Shay, T.; Duarte, F. Tunable fiber lasers. In *Tunable Laser Applications*; CRC Press: Boca Raton, FL, USA, 2009 ; pp. 179–196.
5. Pisarchik, A.; Jaimes-Reátegui, R.; Sevilla-Escoboza, R.; García-Lopez, J.; Kazantsev, V. Optical fiber synaptic sensor. *Opt. Lasers Eng.* **2011**, *49*, 736–742. [CrossRef]
6. Mary, R.; Choudhury, D.; Kar, A.K. Applications of fiber lasers for the development of compact photonic devices. *IEEE J. Sel. Top. Quantum Electron.* **2014**, *20*, 72–84. [CrossRef]
7. Zhao, L.; Li, D.; Li, L.; Wang, X.; Geng, Y.; Shen, D.; Su, L. Route to larger pulse energy in ultrafast fiber lasers. *IEEE J. Sel. Top. Quantum Electron.* **2017**, *24*, 1–9. [CrossRef]
8. Jaimes-Reátegui, R.; Esqueda de la Torre, J.O.; García-López, J.H.; Huerta-Cuellar, G.; Aboites, V.; Pisarchik, A.N. Generation of giant periodic pulses in the array of erbium-doped fiber lasers by controlling multistability. *Opt. Commun.* **2020**, *477*, 126355. [CrossRef]
9. Hargrove, L.; Fork, R.L.; Pollack, M. Locking of He–Ne laser modes induced by synchronous intracavity modulation. *Appl. Phys. Lett.* **1964**, *5*, 4–5. [CrossRef]
10. Okhotnikov, O.; Grudinin, A.; Pessa, M. Ultra-fast fibre laser systems based on SESAM technology: New horizons and applications. *New J. Phys.* **2004**, *6*, 177. [CrossRef]
11. Zhang, H.; Tang, D.; Zhao, L.; Tam, H.Y. Induced solitons formed by cross-polarization coupling in a birefringent cavity fiber laser. *Opt. Lett.* **2008**, *33*, 2317–2319. [CrossRef]
12. Matsas, V.; Newson, T.; Richardson, D.; Payne, D.N. Self-starting, passively mode-locked fibre ring soliton laser exploiting non-linear polarisation rotation. *Electron. Lett.* **1992**, *28*, 1391–1393. [CrossRef]
13. Zhao, L.; Tang, D.; Wu, J. Gain-guided soliton in a positive group-dispersion fiber laser. *Opt. Lett.* **2006**, *31*, 1788–1790. [CrossRef] [PubMed]
14. Yun, L.; Liu, X.; Mao, D. Observation of dual-wavelength dissipative solitons in a figure-eight erbium-doped fiber laser. *Opt. Express* **2012**, *20*, 20992–20997. [CrossRef] [PubMed]
15. Richardson, D.J.; Laming, R.I.; Payne, D.N.; Matsas, V.; Phillips, M.W. Self-starting, passively mode-locked erbium fibre ring laser based on the amplifying Sagnac switch. *Electron. Lett.* **1991**, *27*, 542–544. [CrossRef]
16. Castillo-Guzmán, A.; Anzueto-Sánchez, G.; Selvas-Aguilar, R.; Estudillo-Ayala, J.; Rojas-Laguna, R.; May-Arrioja, D.; Martínez-Ríos, A. Erbium-doped tunable fiber laser. In Proceedings of the Laser Beam Shaping IX, San Diego, CA, USA, 11–12 August 2008; International Society for Optics and Photonics: Bellingham, WA, USA, 2008; Volume 7062, p. 70620Y.
17. Saucedo-Solorio, J.M.; Pisarchik, A.N.; Kir'yanov, A.V.; Aboites, V. Generalized multistability in a fiber laser with modulated losses. *JOSA B* **2003**, *20*, 490–496. [CrossRef]
18. Reategui, R.; Kir'yanov, A.; Pisarchik, A.; Barmenkov, Y.O.; Il'ichev, N. Experimental study and modeling of coexisting attractors and bifurcations in an erbium-doped fiber laser with diode-pump modulation. *Laser Phys.* **2004**, *14*, 1277–1281.
19. Ke, J.; Yi, L.; Xia, G.; Hu, W. Chaotic optical communications over 100-km fiber transmission at 30-Gb/s bit rate. *Opt. Lett.* **2018**, *43*, 1323–1326. [CrossRef]

20. Lim, H.; Jiang, Y.; Wang, Y.; Huang, Y.C.; Chen, Z.; Wise, F.W. Ultrahigh-resolution optical coherence tomography with a fiber laser source at 1 µm. *Opt. Lett.* **2005**, *30*, 1171–1173. [CrossRef]

21. Keren, S.; Horowitz, M. Interrogation of fiber gratings by use of low-coherence spectral interferometry of noiselike pulses. *Opt. Lett.* **2001**, *26*, 328–330. [CrossRef]

22. Droste, S.; Ycas, G.; Washburn, B.R.; Coddington, I.; Newbury, N.R. Optical frequency comb generation based on erbium fiber lasers. *Nanophotonics* **2016**, *5*, 196–213. [CrossRef]

23. Wu, Q.; Okabe, Y.; Sun, J. Investigation of dynamic properties of erbium fiber laser for ultrasonic sensing. *Opt. Express* **2014**, *22*, 8405–8419. [CrossRef]

24. Kraus, M.; Ahmed, M.A.; Michalowski, A.; Voss, A.; Weber, R.; Graf, T. Microdrilling in steel using ultrashort pulsed laser beams with radial and azimuthal polarization. *Opt. Express* **2010**, *18*, 22305–22313. [CrossRef] [PubMed]

25. Philippov, V.; Codemard, C.; Jeong, Y.; Alegria, C.; Sahu, J.K.; Nilsson, J.; Pearson, G.N. High-energy in-fiber pulse amplification for coherent lidar applications. *Opt. Lett.* **2004**, *29*, 2590–2592. [CrossRef] [PubMed]

26. Morin, F.; Druon, F.; Hanna, M.; Georges, P. Microjoule femtosecond fiber laser at 1.6 µm for corneal surgery applications. *Opt. Lett.* **2009**, *34*, 1991–1993. [CrossRef] [PubMed]

27. Strogatz, S.H.; Stewart, I. Coupled oscillators and biological synchronization. *Sci. Am.* **1993**, *269*, 102–109. [CrossRef]

28. Boccaletti, S.; Latora, V.; Moreno, Y.; Chavez, M.; Hwang, D.U. Complex networks: Structure and dynamics. *Phys. Rep.* **2006**, *424*, 175–308. [CrossRef]

29. Ermentrout, G. The behavior of rings of coupled oscillators. *J. Math. Biol.* **1985**, *23*, 55–74. [CrossRef]

30. Keener, J.P. Propagation and its failure in coupled systems of discrete excitable cells. *SIAM J. Appl. Math.* **1987**, *47*, 556–572. [CrossRef]

31. Yamauchi, M.; Wada, M.; Nishio, Y.; Ushida, A. Wave propagation phenomena of phase states in oscillators coupled by inductors as a ladder. *IEICE Trans. Fundam. Electron. Commun. Comput. Sci.* **1999**, *82*, 2592–2598.

32. Van der Sande, G.; Soriano, M.C.; Fischer, I.; Mirasso, C.R. Dynamics, correlation scaling, and synchronization behavior in rings of delay-coupled oscillators. *Phys. Rev. E* **2008**, *77*, 055202. [CrossRef]

33. Cohen, D.S.; Neu, J.C.; Rosales, R.R. Rotating spiral wave solutions of reaction-diffusion equations. *SIAM J. Appl. Math.* **1978**, *35*, 536–547. [CrossRef]

34. Noszticzius, Z.; Horsthemke, W.; McCormick, W.; Swinney, H.L.; Tam, W. Sustained chemical waves in an annular gel reactor: A chemical pinwheel. *Nature* **1987**, *329*, 619–620. [CrossRef]

35. Nekorkin, V.I.; Makarov, V.A.; Velarde, M.G. Spatial disorder and waves in a ring chain of bistable oscillators. *Int. J. Bifurc. Chaos* **1996**, *6*, 1845–1858. [CrossRef]

36. Ahmad, H.; Ruslan, N.; Ismail, M.A.; Ali, Z.; Reduan, S.; Lee, C.; Harun, S.W. Silver nanoparticle-film based saturable absorber for passively Q-switched erbium-doped fiber laser (EDFL) in ring cavity configuration. *Laser Phys.* **2016**, *26*, 095103. [CrossRef]

37. Perlikowski, P.; Yanchuk, S.; Wolfrum, M.; Stefanski, A.; Mosiolek, P.; Kapitaniak, T. Routes to complex dynamics in a ring of unidirectionally coupled systems. *Chaos Interdiscip. J. Nonlinear Sci.* **2010**, *20*, 013111. [CrossRef]

38. Matias, M.; Pérez-Muñuzuri, V.; Lorenzo, M.; Marino, I.; Pérez-Villar, V. Observation of a fast rotating wave in rings of coupled chaotic oscillators. *Phys. Rev. Lett.* **1997**, *78*, 219. [CrossRef]

39. Sánchez, E.; Matías, M.A. Transition to chaotic rotating waves in arrays of coupled Lorenz oscillators. *Int. J. Bifurc. Chaos* **1999**, *9*, 2335–2343. [CrossRef]

40. Horikawa, Y. Metastable and chaotic transient rotating waves in a ring of unidirectionally coupled bistable Lorenz systems. *Phys. D Nonlinear Phenom.* **2013**, *261*, 8–18. [CrossRef]

41. Bashkirtseva, I.A.; Ryashko, L.B.; Pisarchik, A.N. Ring of map-based neural oscillators: From order to chaos and back. *Chaos, Solitons Fractals* **2020**, *136*, 109830. [CrossRef]

42. Barba-Franco, J.; Gallegos, A.; Jaimes-Reátegui, R.; Gerasimova, S.; Pisarchik, A. Dynamics of a ring of three unidirectionally coupled Duffing oscillators with time-dependent damping. *Europhys. Lett.* **2021**, *134*, 30005. [CrossRef]

43. Sánchez, E.; Pazó, D.; Matías, M.A. Experimental study of the transitions between synchronous chaos and a periodic rotating wave. *Chaos Interdiscip. J. Nonlinear Sci.* **2006**, *16*, 033122. [CrossRef]

44. Arecchi, F.T.; Harrison, R.G. *Instabilities and Chaos in Quantum Optics*; Springer Science & Business Media: Berlin/Heidelberg, Germany, 2012; Volume 34.

45. Pisarchik, A.N.; Kir'yanov, A.V.; Barmenkov, Y.O.; Jaimes-Reátegui, R. Dynamics of an erbium-doped fiber laser with pump modulation: Theory and experiment. *JOSA B* **2005**, *22*, 2107–2114. [CrossRef]

46. Pisarchik, A.N.; Jaimes-Reátegui, R.; Sevilla-Escoboza, R.; Huerta-Cuellar, G.; Taki, M. Rogue waves in a multistable system. *Phys. Rev. Lett.* **2011**, *107*, 274101. [CrossRef]

47. Huerta-Cuellar, G.; Pisarchik, A.; Kir'yanov, A.; Barmenkov, Y.O.; del Valle Hernández, J. Prebifurcation noise amplification in a fiber laser. *Phys. Rev. E* **2009**, *79*, 036204. [CrossRef] [PubMed]

48. Bibi, S.; Huerta-Cuellar, G.; Echenausía-Monroy, J.L.; Jaimes-Reátegui, R.; García-López, J.H.; Pisarchik, A.N. Harnessing Multistability: A Novel Approach to Optical Logic Gate Construction Using Erbium-Doped Fiber Lasers. *Photonics* **2024**, *11*, 176. [CrossRef]

49. Pisarchik, A.N.; Barmenkov, Y.O.; Kir'yanov, A.V. Experimental characterization of the bifurcation structure in an erbium-doped fiber laser with pump modulation. *IEEE J. Quantum Electron.* **2003**, *39*, 1567–1571. [CrossRef]

50. Alon, U. Network motifs: Theory and experimental approaches. *Nat. Rev. Genet.* **2007**, *8*, 450–461. [CrossRef]

51. Boccaletti, S.; Pisarchik, A.N.; Del Genio, C.I.; Amann, A. *Synchronization: From Coupled Systems to Complex Networks*; Cambridge University Press: Cambridge, UK, 2018.

52. Jaimes-Reategui, R. Dynamic of Complex System with Parametric Modulation: Duffing Oscillators and a Fiber Laser. Ph.D. Thesis, Centro de Investigaciones en Optica, León de los Aldama, Mexico, 2004.

53. Barba-Franco, J.; Romo-Muñoz, L.; Jaimes-Reátegui, R.; García-López, J.; Huerta-Cuellar, G.; Pisarchik, A. Electronic equivalent of a pump-modulated erbium-doped fiber laser. *Integration* **2023**, *89*, 106–113. [CrossRef]

54. Landau, L.D. On the problem of turbulence. *C. R. Acad. Sci. URSS* **1944**, *44*, 311. [CrossRef]

55. Hopf, E. A mathematical example displaying features of turbulence. *Commun. Pure Appl. Math.* **1948**, *1*, 303–322. [CrossRef]

56. Newhouse, S.; Ruelle, D.; Takens, F. Occurrence of strange axiom A attractors near quasi periodic flows on T^m, $m \geqq 3$. *Commun. Math. Phys.* **1978**, *64*, 35–40. [CrossRef]

57. Matias, M.; Güémez, J.; Pérez-Munuzuri, V.; Marino, I.; Lorenzo, M.; Pérez-Villar, V. Size instabilities in rings of chaotic synchronized systems. *Europhys. Lett.* **1997**, *37*, 379. [CrossRef]

58. Marino, I.; Pérez-Muñuzuri, V.; Pérez-Villar, V.; Sánchez, E.; Matias, M. Interaction of chaotic rotating waves in coupled rings of chaotic cells. *Phys. D Nonlinear Phenom.* **1999**, *128*, 224–235. [CrossRef]

59. Matías, M.; Güémez, J. Transient periodic rotating waves and fast propagation of synchronization in linear arrays of chaotic systems. *Phys. Rev. Lett.* **1998**, *81*, 4124. [CrossRef]

60. Borkowski, L.; Perlikowski, P.; Kapitaniak, T.; Stefanski, A. Experimental observation of three-frequency quasiperiodic solution in a ring of unidirectionally coupled oscillators. *Phys. Rev. E* **2015**, *91*, 062906. [CrossRef]

61. Borkowski, L.; Stefanski, A. Stability of the 3-torus solution in a ring of coupled Duffing oscillators. *Eur. Phys. J. Spec. Top.* **2020**, *229*, 2249–2259. [CrossRef]

62. Barba-Franco, J.; Gallegos, A.; Jaimes-Reátegui, R.; Muñoz-Maciel, J.; Pisarchik, A. Dynamics of coexisting rotating waves in unidirectional rings of bistable Duffing oscillators. *Chaos Interdiscip. J. Nonlinear Sci.* **2023**, *33*, 073126. [CrossRef]

63. Krysko, A.; Awrejcewicz, J.; Papkova, I.; Krysko, V. Routes to chaos in continuous mechanical systems: Part 2. Modelling transitions from regular to chaotic dynamics. *Chaos Solitons Fractals* **2012**, *45*, 709–720. [CrossRef]

64. Awrejcewicz, J.; Krysko, A.; Papkova, I.; Krysko, V. Routes to chaos in continuous mechanical systems. Part 3: The Lyapunov exponents, hyper, hyper-hyper and spatial–temporal chaos. *Chaos Solitons Fractals* **2012**, *45*, 721–736. [CrossRef]

65. Borkowski, L.; Stefanski, A. FFT bifurcation analysis of routes to chaos via quasiperiodic solutions. *Math. Probl. Eng.* **2015**, *2015*, 367036. [CrossRef]

66. Barba-Franco, J.; Gallegos, A.; Jaimes-Reátegui, R.; Pisarchik, A. Dynamics of a ring of three fractional-order Duffing oscillators. *Chaos Solitons Fractals* **2022**, *155*, 111747. [CrossRef]

67. Pisarchik, A.; Jaimes-Reategui, R. Control of basins of attraction in a multistable fiber laser. *Phys. Lett. A* **2009**, *374*, 228–234. [CrossRef]

68. Meucci, R.; Marc Ginoux, J.; Mehrabbeik, M.; Jafari, S.; Clinton Sprott, J. Generalized multistability and its control in a laser. *Chaos Interdiscip. J. Nonlinear Sci.* **2022**, *32*, 083111. [CrossRef] [PubMed]